IOP Publishing Biofabrication 18 (2026) 015025 https://doi.org/10.1088/1758-5090/ae288d

Biofabrication

PAPER

Rescue of extreme hepatectomy mice by primary hepatocyte-derived 3D bio-printed organ transplantation

Bao Jin[1,7], **Zhibo Xie**[1,7], **Yinhan Wang**[1,7], **Yuce Lu**[1,7], **Lejia Sun**[1,2,3], **Zhangyuting He**[1], **Yuqian Ye**[1,4], **Zhiyuan Fang**[1], **Yarong Chi**[1], **Mingchang Pang**[1], **Changcan Li**[1], **Hang Sun**[1], **Zhuoran Danny Jiang**[5], **Xindi Ke**[1], **Haifeng Xu**[1], **Haitao Zhao**[1], **Xinting Sang**[1], **Shunda Du**[1], **Pengyu Huang**[6,*], **Huayu Yang**[1,*] and **Yilei Mao**[1,*]

[1] Department of Liver Surgery, Peking Union Medical College Hospital (PUMCH), Chinese Academy of Medical Sciences (CAMS) & Peking Union Medical College (PUMC), Beijing, People's Republic of China
[2] Department of General Surgery, The First Affiliated Hospital, Nanjing Medical University, Nanjing, People's Republic of China
[3] The First School of Clinical Medicine, Nanjing Medical University, Nanjing, People's Republic of China
[4] Department of Head and Neck Surgery, National Cancer Center/National Clinical Research Center for Cancer/Cancer Hospital, Chinese Academy of Medical Sciences and Peking Union Medical College, Beijing, People's Republic of China
[5] Institute of Biomedical Engineering, Department of Engineering Science, University of Oxford, Oxford, OX3 7DQ, United Kingdom
[6] Institute of Biomedical Engineering, Chinese Academy of Medical Sciences and Peking Union Medical College, Tianjin, People's Republic of China
[7] Bao Jin, Zhibo Xie, Yinhan Wang and Yuce Lu contributed equally to this work.
[*] Authors to whom any correspondence should be addressed.

E-mail: huangpengyu@yeah.net, dolphinyahy@hotmail.com and pumch-liver@hotmail.com

OPEN ACCESS

RECEIVED
10 January 2025

REVISED
17 November 2025

ACCEPTED FOR PUBLICATION
5 December 2025

PUBLISHED
13 January 2026

Keywords: 3D bioprinting, primary mouse hepatocytes, extreme hepatectomy, acute liver failure, liver zonation

Supplementary material for this article is available online

Abstract

Three-dimensional (3D) bioprinting is an emerging strategy for constructing tissues and organs *in vitro*. Here, we achieved long-term expansion of primary mouse hepatocytes using a defined medium and constructed liver tissue using 3D bioprinting. The 3D-printed liver tissue demonstrated several essential liver functions and was able to prolong the survival of mice with acute liver failure due to extreme hepatectomy after *in vivo* transplantation, and the transplanted artificial liver tissue showed distinct functional partitioning. Overall, our results develop a method for long-term *in vitro* culture of primary hepatocytes and demonstrate the potential of 3D bio-printed liver tissue for clinical translational applications.

1. Introduction

The liver is an extremely important and complex metabolic organ. Although it has a strong regenerative capacity, it can be greatly limited under certain pathological conditions [1, 2]. For patients with liver failure, liver transplantation is a viable solution; however, the shortage of donor organs is becoming increasingly problematic [3, 4]. In addition, bioartificial liver (BAL) and cellular therapies have the disadvantages of low hepatocyte function, complex technology, and high cost, so they have not been widely clinically applied [5, 6]. In recent years, *in vitro* biomanufacturing techniques have made some research progress in constructing liver tissues for liver function repair and replacement [7, 8].

Three-dimensional (3D) bioprinting technology is one of the most advanced core technologies *in vitro* biomanufacturing, which can precisely control the spatial distribution of cells and the surrounding microenvironments to construct *in vitro* tissues and 2 organs with complex structures and biological functions [9, 10]. Currently, some *in vitro* tissues and organs, such as the heart and lung, have been constructed based on 3D bioprinting technology [11, 12], and our previous studies have successfully achieved the construction and application of liver tissues [13]. However, there are still many technical hurdles to overcome in this field.

First, there is a lack of easily cultured and good functional hepatocytes. Primary hepatocytes are the best choice for constructing *in vitro* liver tissues

and available replacements. However, their long-term *in vitro* culture faces significant challenges. Recently, Zhang *et al* [14] and Xiang *et al* [15] achieved *in vitro* culture of primary human hepatocytes, but the *in vitro* culture time only lasted 1–2 months, and the cell function rapidly decreased. Peng *et al* [16] and Hu *et al* [17] achieved *in vitro* culture of primary mouse hepatocytes (PMHs) based on organoid technology, but the cell number was unsatisfactory. Although previous studies have reported long-term culture systems for PMHs in two-dimensional (2D) conditions [18–20], obtaining a stable, large-scale cell source suitable for subsequent tissue engineering remains an ongoing challenge.

Second, can the *in vivo* liver function demonstrated by 3D bio-printed liver tissue rescue mice with liver failure? Our previous research confirmed that 3D bio-printed liver tissue exhibits superior therapeutic efficacy in mice with chronic liver failure. [13] However, due to the greater difficulty in treating acute liver failure (ALF), few studies have explored the rescue effect of artificial liver tissue on mice with ALF. Although Deng *et al* recently succeeded in constructing implantable liver tissue using decellularized liver scaffolds and demonstrated its therapeutic potential in a 90% hepatectomy model [21], the field continues to explore diverse technical approaches to optimize functionality and clinical translation feasibility. Deng *et al's* work excellently demonstrates the efficacy of a 'top–down' strategy based on the natural organ extracellular matrix. However, this approach faces challenges in standardizing manufacturing processes, achieving precise microstructural control, and mitigating batch variability in animal-derived materials. In contrast, the 'bottom–up' construction strategy based on 3D bioprinting exhibits unique advantages in precisely controlling the spatial distribution of cells and biomaterials and customizing complex biomimetic structures.

We report the construction of functional liver tissue using 3D bioprinting technology with primary hepatocytes expanded *in vitro* over extended periods. We systematically evaluated its post-transplantation survival and therapeutic efficacy in a model of ALF induced by 90% hepatectomy.

2. Materials and methods

2.1. PMHs isolation and culture

Primary hepatocytes were isolated from C57BL/6 mice by a two-step collagenase perfusion technique with minor modifications. [16] Briefly, insert the catheter into the inferior vena cava, then immediately cut off the portal vein, and perfuse the pre-warmed liver perfusion medium (Gibco, cat. 17701038) through the inferior vena cava into the liver at a rate of approximately 6–8 ml min^{-1} for 5 min. Then, perfuse the pre-warmed digestion medium containing 0.5 mg ml^{-1} collagenase type I (Sigma, cat. C0130) at a rate of 5–6 ml min^{-1} for 5 min. After the liver was digested, it was cut into small pieces and filtered through a 70 μm filter. Hepatocytes were separated from other cells by low-speed centrifugation (50 g $\times$ 5 min).

The isolated hepatocytes were resuspended in RPMI 1640 media (HyClone, cat. SH30027.01) containing 10% fetal bovine serum and seeded on a cell culture dish coated with rat tail collagen I (Gibco, cat. A1048301) in advance at a density of 2×10^4 cm^{-2}. After 6 h, the un-adherent hepatocytes were removed, and the medium was replaced with YACD medium consisting of Advanced DMEM/F12, 2 g l^{-1} galactose, 1% insulin–transferrin–sodium selenite (ITS), 0.3 g l^{-1} proline, 0.61 g l^{-1} nicotinamide, 0.1 g l^{-1} ornithine, 40 ng ml^{-1} transforming growth factor-alpha (TGF-α), 40 ng ml^{-1} epidermal growth factor (EGF), 10 μM dexamethasone (Dex), 10 μM Y-27 632, 0.5 μM A-83-01, 3 μM CHIR99021 and 1% penicillin/streptomycin. During culturing, PMHs were maintained at 37 °C, 5% CO_2 in YACD medium, which was refreshed every 48 h. Hepatocytes are usually passaged with a split ratio of 1:3 every 2–3 d.

2.2. Ethics statement

All experiments involving animals were conducted according to the ethical policies and procedures approved by the Ethics Committee and Institutional Review Board of our hospital (Approval no. XHDW-2023-076).

2.3. 3D bio-printing

The *in vitro* liver constructs were fabricated using two kinds of bio-inks, gelatin–alginate (Gel) and gelatin methacryloyl (GelMA)-LAP, by a 3D bio-printer provided by SUNP Co., following the previously established protocol with appropriate modifications [13, 22]. The 3D bioprinted liver constructs (3DP-LCs) for *in vitro* tests used gelatin–alginate and GelMA-LAP as bio-inks. The 3DP-LCs for *in vivo* transplantation used GelMA-LAP as the bio-ink because of its better structural stability. During printing, the temperature of the nozzle and the printing platform were controlled at 20 °C–22 °C and 10 °C, respectively. The 3DP-LC was a grid-like structure with a size of 10 mm $\times$ 10 mm $\times$ 3 mm, the layer height was 0.25 mm, the line distance was 1.25 mm, the printing speed was 8 mm s^{-1}, and the extrusion speed was 2 mm^3 s^{-1}.

For liver constructs using gelatin–alginate, the harvested mouse hepatocytes were prepared into a cell suspension with an initial concentration of 1×10^7 ml^{-1} and mixed uniformly with the 12% gelatin solution and the 4% sodium alginate solution at a ratio of 2:2:1. The final concentrations of cells, gelatin and sodium alginate were 5×10^6 ml^{-1}, 4.8%, and 0.8%, respectively. The cell/bio-ink mixture was drawn into a 1 ml sterile syringe with a 23 G needle.

This operation needs to be carried out at 37 °C to prevent the bio-ink from turning into a colloidal state. In addition, air bubbles should be avoided. Next, the syringe was placed at 4 °C for 20 min to make the bio-ink into a colloidal state. Subsequently, the syringe was set in a 3D bio-printer (SPP1603) to prepare for fabrication. The liver construct was set as a grid-like structure with a size of 10 mm × 10 mm and a height of 12 layers. The grid-like structure can ensure that the cells have better access to the culture medium. The temperature of the nozzle and molding chamber was adjusted to maintain the highest cell viability during printing. Printing speed, extrusion speed, layer height, line distance, and other parameters were all adjusted to appropriate values to ensure that the bio-ink can be extruded uniformly, and the structure can maintain stability. The withdrawal distance was set to an appropriate value to ensure continuity between layers. The printed structure was collected in a petri dish with a diameter of 35 mm. 3DP-LCs were immersed in 3% calcium chloride solution for 3 min to crosslink with the sodium alginate solution, then the calcium chloride solution was removed, and 3 ml of YACD medium was added.

For liver constructs using GelMA-LAP, the harvested mouse hepatocytes were prepared into a cell suspension with an initial concentration of 1×10^8 ml^{-1} and mixed uniformly with the 12.5% GelMA solution and the 2.5% LAP solution at a ratio of 1:8:1. The final concentrations of cells, GelMA and LAP were 1×10^7 ml^{-1}, 10%, and 0.25%, respectively. The cell/bio-ink mixture was drawn into a 3 ml sterile syringe with a 23 G needle. The mixing process also needs to be carried out at 37 °C to avoid bubbles. Another 3D bio-printer, SunP biomaker, was used to fabricate liver constructs. The structure of liver constructs using GelMA-LAP was set to be the same as that of liver constructs using gelatin–alginate. The light source of SunP biomaker was used for light curing after the liver construct was printed, and the light intensity, light period, and light distance were set to 5%, 20 s, and 10 mm, respectively. Subsequently, 3 ml of YACD medium was added to the petri dish.

2.4. Culture of 2D planar, 3D sandwich and 3DP-LCs

The 2D planar culture was carried out by seeding 1×10^6 cells in a petri dish with a diameter of 60 mm. All 2D planar culture was covered with 3 ml of YACD medium and refreshed every two days. The 3D sandwich culture was performed by seeding 250 μl of cells-gelatin–alginate mixture containing 1×10^6 cells in a 24-well flat-bottom cell culture plate. All 3D sandwich culture was covered with 2 ml of YACD medium and refreshed every two days. All 3DP-LCs were cultured with 3 ml of YACD medium in 35 mm diameter petri dishes and refreshed every two days.

2.5. Cell viability

In order to evaluate the cell survival in 3DP-LCs, a fluorescent live/dead staining was performed to determine the cell viability. Briefly, a mixture of calcein-AM (CAM) (1 μmol l^{-1}, Sigma) and propidium iodide (PI) (2 μmol l^{-1}, Sigma) was prepared in advance. The 3DP-LCs were cross-linked and cured with calcium chloride for 3 min and then washed gently three times with phosphate-buffered saline (PBS) for 1 min. Next, the 3DP-LCs and the prepared CAM/PI mixture were incubated for 15 min at room temperature and protected from light. After incubation, the 3DP-LCs were gently washed with PBS three times and observed under a laser scanning confocal microscope (C2/C2si, Nikon). Cell viability was calculated by counting the number of cells using Image J [(live cell/total cell) × 100%]. Five images of random fields were captured for each sample, and cells in five samples were counted. Cell viability was evaluated on the 0d, 1d, 3d, 5d, 7d, 9d, 11d, 13d, and 15d after printing.

2.6. Cell proliferation

Cell proliferation was measured using cell counting kit-8 (CCK-8) (Dojindo, Japan). Briefly, 2D cells, 3D sandwich cells, and 3DP-LCs were incubated at 37 °C for 4 h in a mixture of culture medium and CCK-8 reagent in a volume ratio of 10:1 at culture days of 0, 1, 3, 5, 7, 9, 11, 13, and 15. After incubation, transfer 110 μl of the mixture into a 96-well plate. The absorbance at 450 nm was measured to determine the cell viability using the microplate reader (AS-AMR-100-1122, Allsheng, China). The data are representative of three independent experiments in triplicate. A standard curve of fluorescence for a certain number of cells at different times was established. The detected fluorescence of the sample was then normalized to cell number according to the standard curve.

2.7. Immunofluorescence

For immunofluorescence staining, the cells were fixed with 4% paraformaldehyde for 20 min at room temperature, and then incubated with PBS containing 0.2% Triton X-100 (Sigma) for 30 min. Cells were then washed three times with PBS. After being blocked by 3% bovine serum albumin (BSA) in PBS for 45 min at room temperature, cells were incubated with primary antibodies at 4 °C overnight, washed three times with PBS, and then incubated with appropriate fluorescence-conjugated secondary antibody for 60 min at room temperature in the dark. Nuclei were stained with DAPI (Sigma). Primary and secondary antibodies were diluted in PBS containing 3% BSA. Primary antibodies used for immunofluorescence are as follows: chicken anti-albumin (1:100; Abcam), mouse anti-E-Cadherin (1:100; BD Transduction Laboratories), mouse anti-AAT (H-7) (1:100; Santa Cruz), mouse anti-CYP3A11 (1:200; Santa Cruz), rabbit anti-GST (1:200; Abcam), and

mouse anti-CD31 (1:100; Abcam). Secondary antibodies used for immunofluorescence are as follows: goat anti-chicken IgG Alexa Fluor 594 (1:500; Abcam), goat anti-mouse IgG Alexa Fluor 488 (1:500; Abcam), goat anti-mouse IgG Alexa Fluor 594 (1:500; Abcam), goat anti-rabbit IgG Alexa Fluor 594 (1:500; Abcam). The laser scanning confocal microscope (C2/C2si, Nikon) was used to observe the stained cells.

2.8. Histology and immunohistochemistry

Specimens were fixed in 4% paraformaldehyde (formalin) and embedded in paraffin using standard procedures. Embedded specimens were cut into 5 μm-thick paraffin slices for hematoxylin and eosin staining (HE) and immunohistochemistry. Tissue sections were stained with hematoxylin and eosin for pathological evaluation. For immunohistological staining, paraffin slices were deparaffinized and dehydrated using xylene and pure ethanol. Slices were then immersed in Ethylenediaminetetraacetic acid (EDTA) antigen retrieval solution (pH 8.0). Slides were treated in 3% H_2O_2 for 15 min, blocked in 5% normal goat or horse serum in 1% BSA-PBS for 20 min, and stained with the indicated antibodies in 1% BSA-PBS overnight. Secondary antibodies were used according to Vectastain ABC kits (Vector Laboratories), followed by DAB staining (DAKO). The following antibodies were used for immunohistochemical staining: rabbit anti-CD31 (Servicebio, GB113151, 1:300), goat anti-mouse albumin (Bethyl Laboratories, A90-134 A, 1:200), chicken anti-albumin (Abcam, ab106582, 1:200), rabbit anti-CPS1 (Abcam, ab45956, 1: 200), rabbit anti-glutamine synthetase (Abcam, ab73593, 1:200), rabbit anti-CYP2 $\times$ 10^1 (Sigma, HPA009128, 1:200), and mouse anti-E-cadherin (BD Transduction Laboratories, 610182, 1:200).

2.9. CYP induction

For the measurement of CYP enzyme induction, 3DP-LCs were cultured in a YACD medium for 7 d and then changed to a YACD medium supplemented with 3-methylcholanthrene (25 μM) for 48 h, rifampicin (25 μM), sodium phenobarbital (2 mM), carbamazepine (100 μM), and acetaminophen (100 μM) for 72 h. Total RNA of cells with and without inducer treatment was extracted to measure the expression of *Cyp450* genes. The gene expression levels of *Cyp1a1, Cyp1a2, Cyp2a6, Cyp2b1, Cyp2b6, Cyp2c8, Cyp2c9, Cyp2d6, Cyp3a11*, and *Cyp2 $\times$ 10^1* were measured by qPCR.

2.10. PAS and DiI-ac-LDL staining, and the ICG uptake assay

Cells were stained by periodic acid-Schiff (PAS, Sigma) and DiI-ac-LDL (Invitrogen) following the manufacturer's instructions. For the indocyanine green (ICG, Sigma) uptake assay, cells were incubated in the medium supplemented with ICG (1 mg ml^{-1}) at 37 °C for 1 h, followed by washing with PBS three times. After 6 h, the excretion of ICG was observed.

2.11. RNA isolation and RT-qPCR

Total RNA was isolated from cells by Trizol (Invitrogen) following the manufacturer's instructions. Subsequent purity, integrity, and degradation evaluation of RNA were performed. One microgram of RNA was reverse transcribed using a ReverTra Ace qPCR RT Master Mix with gDNA Remover Kit (Toyobo) in a 20 μl reaction. After a 20-fold dilution, 4 μl of complementary DNA was used as the template in a 20 μl real-time polymerase chain reaction. For real-time polymerase chain reaction, amplification was performed for 40 cycles using EvaGreen 2X qPCR MasterMix (Applied Biological Materials Inc., Canada). Primers were designed using exon junctions to prevent co-amplification of complementary genomic DNA (supplementary table 1).

2.12. *In vivo* experiment

Mice were divided into four groups in the *in vivo* experiment, each receiving different surgical procedures. Mice in the Sham group underwent simple open and closed abdominal surgery on day 0, and extreme hepatectomy (90% liver resection) on day 7. Mice in the cell-free 3DP transplantation (cf-3DPT) group were transplanted with 3DP-LCs without hepatocytes on day 0, and underwent extreme liver resection on day 7. Mice in the intrasplenic injection (ISI) group received intrasplenic transplantation of PMH on day 0 and underwent extreme liver resection on day 7. Mice in the 3DPT group were transplanted with 3DP-LCs containing hepatocytes on day 0 and underwent extreme liver resection on day 7.

For intrasplenic hepatocyte transplantation, a small incision was made in the flank, and the spleen was exposed. PMH (1×10^6 cells) suspended in 50 μl of HBSS (Gibco™, 14025092) were kept on ice before injection into the spleen of the mouse using a 30-gauge needle, as previously described [23, 24]. For liver resection in mice, we performed a 90% hepatectomy. The procedure follows the method established by Myronovych *et al* [25], that is, a single ligature is used to remove the left lateral, left median, and right median lobes, then the right lateral lobe is excised, leaving only the caudate lobe (10%). For the transplantation of 3DP-LCs, we opened the abdominal cavity of the mice and placed the 3D printed liver tissues in the iliac fossa on both sides. All operations were performed under anesthesia with 1% sodium pentobarbital.

2.13. Liver function assay of mouse serum

Blood samples from mice were collected at various time points and centrifuged at 300 g for 15 min. Albumin, total protein, bilirubin, alanine

aminotransferase, aspartate aminotransferase, lactate dehydrogenase, gamma-glutamyl transpeptidase, alkaline phosphatase, cholinesterase, pre-albumin, and albumin/globulin ratio were estimated using an AU 5800 automated analyzer (Beckmann) in the clinical laboratory of our hospital.

2.14. Single-cell sequencing and analysis

Single-cell sequencing was performed according to official 10x Genomics procedures and standards. 3D-printed liver tissues were removed from the mice 2 weeks after transplantation. Samples were prepared as single-cell suspensions using GelMA lysate (SunP, SP-BI-G04-1). We used the Luna II Cell Counter for cell counting and cell viability determination. The cell viability rate $\geqslant$85% and the cell concentration and total volume $\geqslant 1 \times 10^6$ cells ml^{-1} were considered to meet the requirements. Cell labeling was performed based on the 10x Genomics Chromium TM system. After the library was constructed and passed the quality check, the Illumina NovaSeq6000 platform was used for PE150 sequencing. Sequencing data quality was assessed before starting data analysis. After obtaining high-quality Clean Reads, use 10x Genomics' official analysis software, Cell Ranger, for cell quality control, detection, reference genome comparison, cell cluster analysis, etc.

2.15. Statistical analysis

All data were shown as the mean $\pm$ SD. For most statistical evaluations, a one-sided unpaired Student's *t*-test was applied to calculate statistical probability in this study. For survival analysis, a one-sided Mantel–Cox log-rank test was applied. Statistical analysis was performed employing the Statistical Program for Social Sciences software (IBM). Differences were considered statistically significant if *p*-values were lower than 0.05. For all statistics, data from at least 3 independent samples or repeated experiments were used. No specific statistic calculation was performed to estimate the sample size. Sample sizes were chosen mainly based on previous experience. Details of sample sizes can be found in the figure legends. No samples or animals were excluded from the analysis. All animals were recruited into experimental or control groups randomly by the animal technician. The investigators were not totally blinded to the group allocation in the study.

3. Results

3.1. *In vitro* expansion of PMHs and establishment of 3DP-LCs

We obtained primary hepatocytes from 8-week-old C57BL/6 J male mice by a two-step collagenase perfusion method (figure 1(A)). Only when the total number of hepatocytes isolated from each mouse exceeds 3×10^7, and the viability exceeds 80%, will it be used for subsequent experiments. In 2D culture, the hepatocytes were passaged at a ratio of 1:3, which can be continuously passaged for at least 60 passages (no longer passages were tried), and the cell morphology did not change significantly. Figure 1(B) shows the 60th-passage hepatocytes, while figure S3 displays hepatocytes from the 14th, 19th, 29th, and 55th passages, respectively, indicating that no significant morphological changes occurred in the hepatocytes during serial passage. We performed immunofluorescence staining analysis on PMH cells from the 10th to the 50th passage. The results demonstrated that cells from different passages stably expressed hepatocyte-specific markers such as ALB and AAT (figures S4 and S5). In most cases, the hepatocytes used in experiments were in the 30th to 50th generation.

The schematic process of 3D bioprinting is shown in figure 1(A). The 3D bioprinting protocol was based on our previous studies [13, 26, 27]. On the 0th, 3rd, 5th, 9th, 13th, and 30th days after printing, the general and light microscope morphology of 3DP-LCs was photographed and recorded, and the cell viability was measured (figure 1(C)). We performed quantitative analysis of cell viability using ImageJ. The results showed that over 95% of cells remained viable within two weeks post-printing, and more than 80% of cells were still alive at 30 d post-printing. Figure 1(D) displays the cell proliferation curves of 2D culture, 3D culture, and 3D printing (3DP) culture, as determined by CCK-8 assay results. Hepatocytes in 2D state had the fastest proliferation rate, while 3D culture and 3DP culture had almost no proliferation.

3.2. *In vitro* liver function testing of 3DP-LCs

We analyzed the expression of liver-specific genes in the PMH group, 2D group, 3D group, and 3DP group by qPCR detection. Compared with the 2D and 3D groups, the hepatocytes of the 3DP group expressed the highest levels of genes related to liver function, including *Albumin* (*Alb*), *Alpha1-antitrypsin* (*Aat*), *ferroportin*, and *Asialoglycoprotein receptor 1* (*Asgr1*) (figure 2(A)). The expression levels of some genes in the 3DP group even exceeded those in the PMH group, such as *Cytokeratin 8* (*Ck8*), *Cytokeratin 18* (*Ck18*), *Multidrug resistance protein 2* (*Mrp2*), and *Farnesoid X receptor* (*Fxr*) (figure 2(B)). The expression profiles of other liver-specific genes are shown in figure S1(A).

We measured albumin concentrations in the culture supernatants of the 2D culture group, 3D culture group, and 3D-printed group at different time points using clinical laboratory testing methods. The results showed that hepatocytes in all three groups exhibited robust albumin secretion capacity. Notably, the albumin concentration in the supernatant of the 3D-printed group reached a significant peak detectable after day 5 of culture, surpassing that of the other two groups (figure S6).

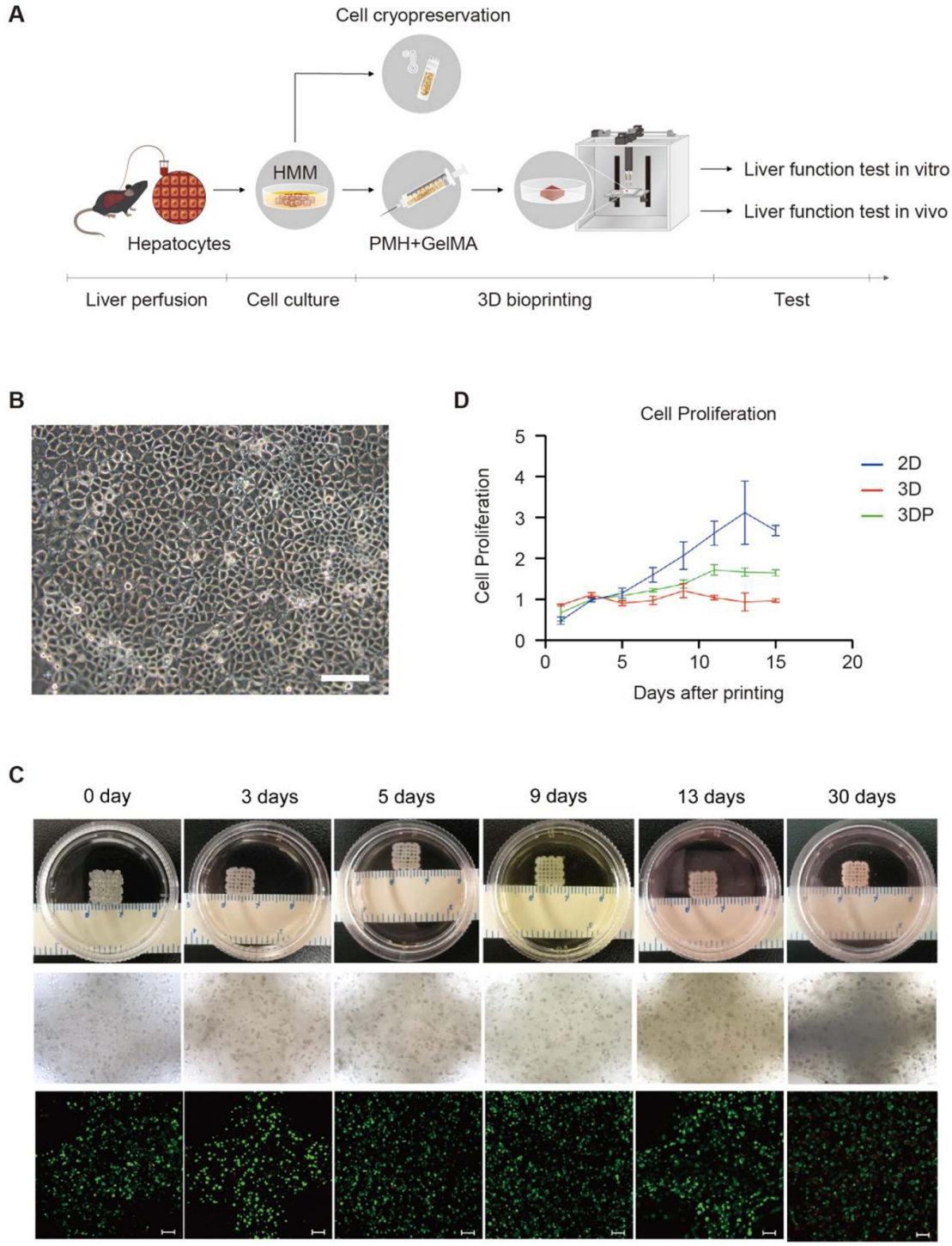

Figure 1. Fabrication and culture of the three-dimensional bio-printed liver constructs (3DP-LCs). (A) Primary mouse hepatocytes were isolated, cultured, and expanded, and 3DP-LCs were constructed using a 3D bio-printer. Subsequently, 3DP-LCs were tested for liver function *in vitro* and *in vivo*. (B) Primary mouse hepatocytes cultured *in vitro* (passage 60). Scale bar = 100 μm. (C) General morphology, light microscopic morphology, and live/dead staining of 3DP-LCs on days 0, 3, 5, 9, 13, and 30 after printing. (D) Cell proliferation in 2D planar, 3D sandwich, and 3DP-LCs cultures. Scale bar = 100 μm.

In order to detect the drug metabolism function of 3DP-LCs, we conducted a CYP450 enzyme drug induction experiment. We used five drugs, including rifampicin, phenobarbital, 3-methylcholanthrene, carbamazepine, and acetaminophen, for the experiment. Rifampicin, phenobarbital, and 3-methylcholanthrene induced an increase in the expression of at least one CYP450 enzyme (figure 2(C)), while carbamazepine and acetaminophen failed to induce it (figures S1(B) and (C)). The most frequently induced CYP450 enzymes with increased expression levels were CYP1A2, CYP1B1, CYP2A6, and CYP2 $\times$ 10^1.

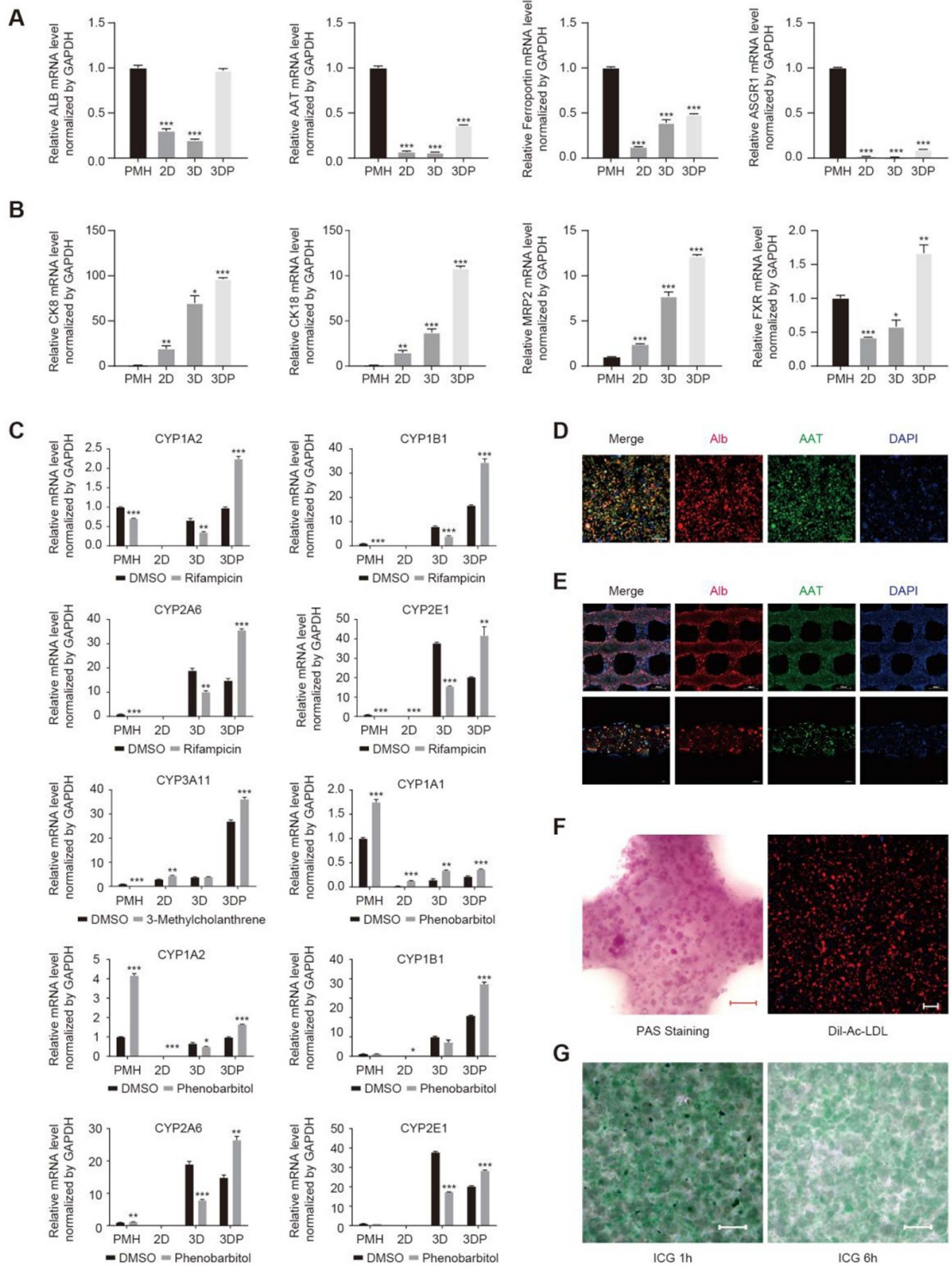

Figure 2. *In vitro* liver function testing of the three-dimensional bio-printed liver constructs (3DP-LCs). (A), (B) Quantitative PCR analysis of hepatic marker gene expression in 3DP-LCs on day 7 after printing. (A) *Alb, Aat, Ferroportin* and *Asgr1*, (B) *Ck8, Ck18, Mrp2*, and *Fxr*. Results are represented as mean ± SD, $n = 3$. (C) Quantitative PCR analysis of CYP450 enzyme gene expression in 3DP-LCs on day 7 after printing. Results are represented as mean ± SD, $n = 3$. (D), (E) The expression of hepatocyte marker proteins ALB (red) and AAT (green) in Gel-3DP-LCs (D) and GelMA-3DP-LCs (E) determined by immunofluorescence staining. The magnification ratios for the upper and lower regions of figure (e) are 40× and 100×, respectively. (F) PAS staining and DiI-ac-LDL uptake in 3DP-LCs. (G) ICG uptake and release in 3DP-LCs. Scale bar = 100 μm. $^{*}P < 0.05$, $^{**}P < 0.01$, $^{***}P < 0.001$.

We further analyzed the expression of hepatocyte-specific proteins of 3DP-LCs through immunofluorescence staining experiments. The results showed that 3DP-LCs had abundant expression of ALB, AAT, CYP3A11, and GST (figures 2(D) and S1(D)). In addition to Gel-3DP-LCs, we also performed immunofluorescence staining analysis on GelMA-3DP-LCs. The results showed that GelMA-3DP-LCs also had abundant expression of albumin and AAT (figure 2(E)).

In addition, we also proved the glycogen storage and low-density lipoprotein uptake functions of 3DP-LCs by PAS staining and DiI-ac-LDL staining (figure 2(F)). The ICG uptake and excretion test is a commonly used clinical test to judge liver function. We conducted ICG uptake and excretion experiments on 3DP-LCs. The results showed that when 3DP-LCs were incubated with 1 mg ml^{-1} ICG for 1 h, 3DP-LCs would take up ICG into the cell, and significant excretion was observed after 6 h (figure 2(G)). The above results fully demonstrated that 3DP-LCs had several important liver functions *in vitro*.

3.3. *In vivo* transplantation of 3DP-LCs

To explore the liver function of 3DP-LCs *in vivo*, we transplanted them into the abdominal cavity of C57BL/6 J mice. Mice were divided into four groups in the *in vivo* experiment, each receiving different surgical procedures, as shown in figure 3(A). In our preliminary investigations, we found that immediate transplantation of 3DP-LCs following 90% hepatectomy failed to improve mouse survival (data not shown). This prompted us to adopt a strategy of transplanting one week before hepatectomy, allowing sufficient time for the graft to undergo vascularization and establish function *in vivo*. We followed up the mice in the above four groups for up to 7 d, recorded their survival time, and drew a Kaplan–Meier survival curve. A total of 84 mice were finally included in the survival analysis, of which 36 were in the sham group, 8 were in the cf-3DPT group, 23 were in the 3DPT group, and 17 were in the ISI group. We found that the survival time of mice in the 3DPT group was significantly longer than that of the sham group ($P = 0.008$), while the survival time of mice in the cf-3DPT group and ISI group was not significantly different from that of mice in the sham group ($P > 0.05$) (figure 3(B)).

The blood samples of the mice in the above four groups were collected for biochemical liver function tests on the first, third, and seventh days after hepatectomy. In addition, we also collected blood samples from mice that did not undergo any intervention. It can be found that on the first day after hepatectomy, the liver function damage indexes (such as ALT, AST, and ALP) of the mice in the 3DPT group were lower than those in the sham, cf-3DPT, and ISI group, although there was no statistically significant difference (figure 3(C)). Considering that we were using an acute liver injury mouse model, the liver function of the mice that can survive to the 3rd day or even the 7th day has been compensated, so there was no significant difference in the liver injury indicators of the three groups of mice (figure 3(C)). We compared the liver function of mice in the same group at different time points, and the results proved that the liver function of mice that could survive more than 3 d had indeed been compensated (figure S2(A)). In terms of protein secretion, the total protein and albumin levels of the mice in the 3DPT group on the first day after hepatectomy were lower than those in the sham, cf-3DPT, and ISI groups (figure 3(C)). The total protein level of mice in the cf-3DPT group and 3DPT group increased over time, while the albumin level did not change significantly (figure S2(A)).

We took out the transplanted 3DP-LCs and residual liver on the 7th day after hepatectomy, the 14th day after 3DP-LCs transplantation. We found that macroscopic vascular connections were formed between the transplanted 3DP-LCs and the abdominal cavity of mice (figure 3(D)). We then performed HE and immunohistochemical (IHC) analysis (figure 3(E)). We confirmed the implantation of new blood vessels of 3DP-LCs transplanted into the body by CD31 staining, which provided the necessary nutrients and oxygen for the survival of hepatocytes in 3DP-LCs. Notably, we found that the liver cells of 3DP-LCs in the body can be partitioned by staining markers such as CPS1, CP2 $\times$ 10^1, and E-CAD that indicate the polarity of liver cells (figure 3(F)).

3.4. Single-cell RNA sequencing analysis of 3DP-LCs after transplantation

We took out the transplanted 3DP-LCs for dissociation on the 7th day after hepatectomy, that is, on the 14th day after the transplantation of 3DP-LCs, and performed single-cell RNA sequencing analysis on the obtained cell suspension. We found that 3DP-LCs *in vivo* had become a tissue containing a variety of cell types, including hepatocytes (53.3%) and macrophages (31.7%), as well as T cells, dendritic cells, endothelial cells, NK cells, monocytes, and B cells (figure 4(A)). In order to further explore whether the hepatocytes of 3DP-LCs *in vivo* were zoned, we analyzed the ALB+ cell population. We found a lot of Glul+ cells, while CPS1+, CYP2 $\times$ 10^1+, and Cdh1+ cells were not obvious (figure 4(B)).

4. Discussion

In recent years, 3D bioprinting has gradually expanded from the printing of only biological materials to the printing of living cells [28]. Due to the advantages of precise control over the spatial arrangement of cells, 3D bioprinting has shown great application potential in the construction of *in vitro* tissues and organs [9, 29, 30]. Based on our previous studies [13, 26, 27], we used expandable PMHs to construct *in vitro* liver tissue using

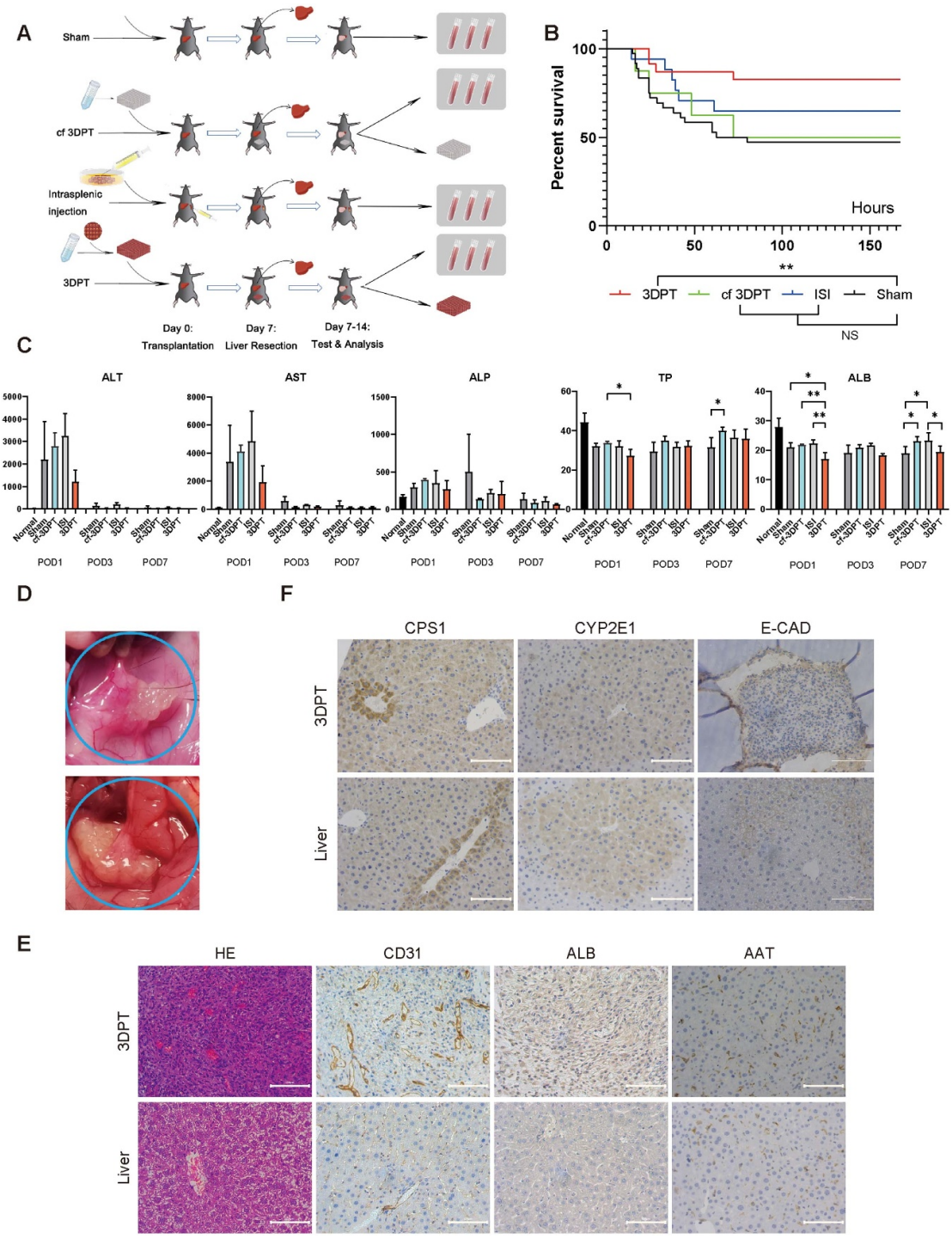

Figure 3. *In vivo* transplantation of the three-dimensional bio-printed liver constructs (3DP-LCs). (A) The groups of mice and the surgical procedures they underwent *in vivo* experiments. (B) Kaplan–Meier survival curve of 3DP-LCs-transplanted (3DPT) group mice ($n = 23$), sham group mice ($n = 36$), cell-free 3DP-LCs-transplanted (cf-3DPT) group mice ($n = 8$), and ISI group mice ($n = 17$). (C) Serum levels of alanine aminotransferase (ALT), aspartate aminotransferase (AST), alkaline phosphatase (ALP), total protein (TP), and albumin (ALB) in different groups of mice. Serum samples were collected on postoperative day (POD) 1, 3, and 7 after hepatectomy. (Normal, $n = 4$; POD1: Sham, $n = 4$; cf-3DPT, $n = 4$; ISI, $n = 4$; 3DPT, $n = 3$; POD3: Sham, $n = 6$; cf-3DPT, $n = 3$; ISI, $n = 2$; 3DPT, $n = 3$; POD7: Sham, $n = 8$; cf-3DPT, $n = 4$; ISI, $n = 5$; 3DPT, $n = 6$). Data are presented as mean ± SD. (D) Macroscopic vascular connections were formed between the transplanted 3DP-LCs and the abdominal cavity of mice. (E), (F) HE staining and immunohistochemical staining of the transplanted 3DP-LCs and residual liver. Scale bar = 100 μm. NS: not significant, $^{*}P < 0.05$, $^{**}P < 0.01$, $^{***}P < 0.001$.

3D bioprinting and demonstrated that it can prolong the survival of mice with ALF induced by extreme hepatectomy. We also found that 3D-printed liver tissue can differentiate into different functional subpopulations of hepatocytes *in vivo*. These findings suggest that 3D printed liver tissue may

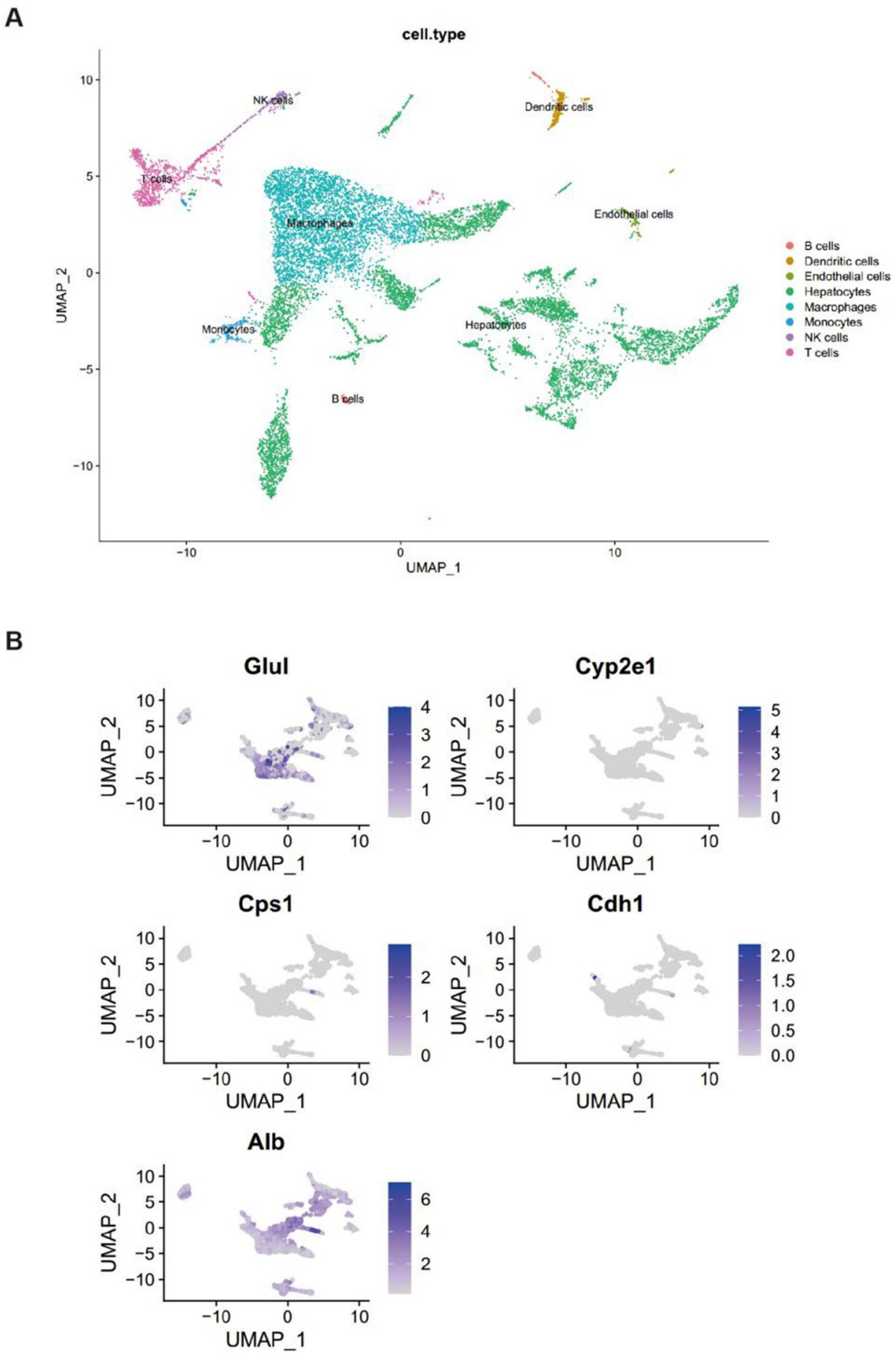

Figure 4. (A) Single-cell RNA sequencing analysis revealed that the transplanted 3DP-LCs had become a tissue containing a variety of cell types. (B) Analysis of ALB-positive cell populations revealed many Glul-positive cell subpopulations.

have crucial potential applications in the treatment of ALF.

Worldwide, the disease burden of various liver diseases is gradually increasing [5, 31, 32]. The only treatment for end-stage liver disease is orthotopic liver transplantation. However, the donor organs are far from meeting clinical needs [33]. To overcome the shortage of donor organs, alternative methods such as cell transplantation, BAL, and engineering liver tissues are emerging. All these alternative therapies require the support of a large number of functional hepatocytes. In recent years, many efforts have been made to expand the source of functional liver cells. Studies have shown that under certain conditions, liver progenitor cells, embryonic stem cells, pluripotent stem cells, fibroblasts, and mesenchymal stem cells have the potential to produce functional liver cells [34–40]. Recently, some studies have described several protocols for long-term expansion of primary hepatocytes *in vitro* [14, 15, 41]. Although these findings have greatly expanded the source of functional hepatocytes, their practical application is subject to many limitations, such as insufficient liver function, complex procedures, and high costs. In this study, we found the culture conditions that can maintain the long-term stable expansion of PMHs *in vitro* by modifying the medium composition. PMHs can be stably passaged to at least the 60th passage, with no obvious changes in cell morphology. Although hepatocytes lost most of their liver function under long-term 2D flat culture conditions, they will regain liver function under 3D culture conditions after 3D bioprinting.

During the printing process, the basic printing parameter settings, including the shape of the print body, the printing temperature, the printing speed, the extrusion speed, and the concentration of the bio-ink, were all in accordance with our previous studies [13, 26, 27]. In this study, we employed two distinct hydrogel systems tailored for specific applications: a gelatin–alginate composite for *in vitro* functionality tests and GelMA-LAP for *in vivo* transplantation. The choice of gelatin–alginate was predicated on its reversible thermal gelation and mild ionic crosslinking, which facilitates easy dissociation for subsequent cellular analysis. For the more demanding *in vivo* environment, we selected GelMA-LAP due to its superior mechanical stability and biocompatibility following photo crosslinking. In the initial animal experiments, we used a gelatin–alginate printing system; however, all the printed bodies transplanted into the abdominal cavity disappeared after 7 d of liver resection. We speculate that this may be due to the activation of a certain enzymatic system in the body by the stress of liver resection, as this phenomenon was not present in the previous study [13] (transplantation only, no liver resection). This problem is solved by using the bio-ink printing system of GelMA-LAP. While a detailed rheological and mechanical characterization of the hydrogel was not the central focus of this work, the high post-printing cell viability, sustained albumin secretion, and the robust expression of mature hepatic markers affirm the suitability of our selected bio-ink formulations for maintaining primary hepatocyte functionality. Furthermore, the successful vascularization and therapeutic efficacy of the GelMA-based constructs *in vivo* underscore their utility for implantation. Future work will benefit from a systematic investigation of hydrogel properties (e.g. stiffness, degradation kinetics, ligand density) to further optimize the functional maturation and spatial organization of bioprinted liver tissues.

Many studies have shown that the 3DP process will not cause substantial damage to cell activity, and cells can maintain good activity for a long time in appropriate bio-inks. In our study, more than 95% of the cells were still alive within 2 weeks of printing. Under normal circumstances, the proliferation rate of hepatocytes cannot be combined with liver function. Under our culture conditions, 2D-cultured hepatocytes proliferated the fastest, while 3D-cultured and 3DP-cultured cells did not proliferate significantly. In the follow-up *in vitro* liver function tests, hepatocytes in the 3DP group showed surprising liver functions, including protein secretion, drug metabolism, glycogen storage, low-density lipoprotein uptake, and ICG uptake and excretion functions. The above aspects of liver function lay the foundation for the printed body to function *in vivo*.

After completing *in vitro* liver function tests, we conducted *in vivo* experiments. The results showed that the 3D printed liver tissue helped the mice survive the ALF period after extreme hepatectomy, extending the overall survival of the mice. Hepatocyte transplantation is considered a promising alternative to liver transplantation for the treatment of metabolic liver disease, ALF, and chronic liver failure, among others [5]. However, an insufficient source of hepatocytes, decreased function, and cell loss after infusion limit its clinical application [42, 43]. In our study, we innovatively used expandable PMHs and successfully constructed liver tissue blocks in combination with 3D bioprinting technology and transplanted them directly into the abdominal cavity of mice to exert liver function. Compared to our previous study [13], we increased the hepatocyte concentration in the liver tissue block to 1×10^7 cells ml^{-1}. Each mouse was transplanted with 2 liver tissue blocks, with a total volume of about 0.5 ml, so the total number of liver cells was 5×10^6. We believe these extra numbers of liver cells can help improve liver function. In addition, the timing of transplantation is also very important. Implantation of the printed body after hepatectomy was ineffective (data not shown) and only effective before hepatectomy. We performed the transplantation one week before hepatectomy to allow sufficient time for the graft to establish a blood supply

and develop functional capacity within the recipient. The primary reason for the higher survival rate of the 3DP-LCs grafted group is believed to be that the graft re-established a vascular system within the mouse body to obtain oxygen and nutrients, thereby partially performing the functions of liver cells *in vivo*. In previous research, Yang *et al* demonstrated that 3D bio-printed liver organoids can prolong the survival of mice with chronic liver failure caused by Fah gene deletion [13]. They observed the formation of new blood vessels derived from the mice within the 3D-printed organoids after transplantation, enabling the printed structures to survive *in vivo* and perform liver functions. Additionally, mechanisms such as the supportive microenvironment provided by the extracellular matrix and potential endogenous liver regeneration may also play a positive role in prolonging survival in mice with ALF.

The most critical finding of this study is that liver tissue constructed from 3D bio-printed and expandable hepatocytes (3DP-LCs) successfully rescued mice undergoing 90% extreme liver resection after heterotopic transplantation. This discovery corroborates the positive therapeutic outcomes recently reported by Deng *et al* using decellularized liver scaffolds [21]. However, the two studies employ fundamentally different technical approaches to achieve this goal, offering complementary insights and options for the field. The decellularized liver scaffold used by Deng *et al* maximally preserves the complex extracellular matrix components and microvascular network template of the native liver, potentially providing an ideal foundation for cellular function maintenance and rapid vascular anastomosis. In contrast, our study demonstrates the equivalent efficacy of a 'bottom–up' strategy combining 3D bioprinting with explicitly defined hydrogels, such as GelMA. Our approach offers potential advantages in manufacturing flexibility, structural customizability, and avoidance of animal organ-derived materials. Although the currently used GelMA remains animal-derived, its synthesis process is more readily standardized than whole-organ decellularization and can seamlessly transition to fully synthetic biomimetic hydrogels to meet stringent clinical translational regulatory requirements. Furthermore, the long-term *in vitro* expanded primary hepatocytes used in our study offer an alternative, promising solution to the fundamental bottleneck of 'cell sourcing' in tissue engineering, compared to primary cells directly isolated from animals. Although functional adaptations occur during hepatocyte expansion, our data unequivocally demonstrate that these cells possess robust redifferentiation and functional maturation capabilities in both 3D-printed and *in vivo* environments. Future efforts may focus on integrating the strengths of different approaches, such as combining printed hepatocyte tissues with pre-vascularized synthetic scaffolds, to further accelerate clinical translation.

Another important finding was that the 3D-printed liver tissue showed signs of liver zonation after transplantation into mice. From the hepatic portal vein area to the hepatic central vein area, hepatocytes can be roughly divided into three zones [44, 45]. Liver zonation plays an important role in maintaining liver homeostasis, regulating liver regeneration, and optimizing overall liver function. Like normal livers, the gradient changes of oxygen, nutrients, and other trace elements caused by the unidirectional flow of blood in the 3D-printed liver tissue may be the reason for the zonation of the hepatocytes in the printed bodies. Single-cell RNA sequencing data revealed a thought-provoking phenomenon: the proportion of glutamine synthetase (Glul)-positive cells in transplanted hepatocytes was significantly higher than the strictly restricted perivascular distribution observed in normal liver tissue. This finding is closely related to the specific physiological state of our construct and may reflect unique biological behaviors during the *in vivo* integration of engineered tissues. We hypothesize that this widespread Glul expression pattern primarily stems from the following factors: First, the transplanted hepatocytes originate from cells expanded *in vitro* over extended periods and undergo the physical stress of 3DP alongside the acute stress of the host environment with liver failure. This series of stimuli may place the cells in a highly activated 'regenerative-like state.' During liver regeneration, metabolic programs undergo reprogramming, and Glul expression undergoes transient de-localization to support the biosynthesis of precursors (e.g. glutamine and nucleotides) required for massive cell proliferation. Thus, the observed high Glul expression may indicate that the transplanted construct as a whole is actively providing metabolic support to the host while maintaining its own survival. Second, this immature partitioning state may relate to the incomplete establishment of morphogen gradients in the early microenvironment of our construct. In a normal liver, the Wnt/β-catenin signaling gradient precisely confines Glul expression to the perivascular region around the central vein. However, in the nascent transplant, although a vascular network has formed (figure 3(E)), it is questionable whether it can mimic such a precise *in vivo* signaling gradient at this early stage. The absence of this spatially restricted signal may lead hepatocytes to exhibit a more homogeneous, highly active metabolic phenotype. In summary, the widespread Glul expression in the transplanted organ is not evidence of functional deficiency. Rather, it likely represents an adaptive or transitional state enabling the engineered tissue to survive, integrate, and function under severe physiological stress. This finding suggests that guiding engineered liver tissue to mature from an effective 'functional mass' into a finely compartmentalized 'organoid' will be a significant challenge and direction for future research.

This study has several distinct innovations from our previous study [13]. First, for cell selection, we used expandable PMHs. The long-term expansion of primary hepatocytes *in vitro* has always been a research difficulty and hotspot. We achieved a large-scale expansion of PMHs by improving the culture medium. Moreover, hepatocytes can differentiate and mature after 3D bioprinting culture and *in vivo* transplantation. Second, in terms of animal models, we used a mouse model of ALF induced by extreme hepatectomy. These results initially demonstrate the potential of 3D printed liver tissue in the treatment of ALF.

Despite the promising therapeutic effects observed in this study, we acknowledge that the pre-hepatectomy transplantation model employed here has inherent limitations in clinical feasibility for treating ALF, as patients typically present after the onset of liver injury. To bridge this gap between proof-of-concept and clinical application, future research must focus on developing strategies for post-injury intervention. A primary and promising direction is the development of 'off-the-shelf,' cryopreservable 3DP-LCs. By optimizing bioink compositions with cryoprotectants (e.g. trehalose, DMSO), we aim to establish robust protocols for the long-term storage and rapid thawing of functional 3D liver constructs. This would enable the immediate availability of 3DP-LCs for emergency transplantation, analogous to the use of banked tissues. Alternatively, the integration of 3DP-LCs into BAL support systems represents a more near-term clinical strategy. In this scenario, the 3DP-LCs would serve as a bioreactor module for temporary extracorporeal liver support, bridging patients to regeneration or transplantation. While the current study establishes the potent efficacy of 3DP-LCs in a stringent model of ALF, we recognize and are committed to overcoming the pivotal hurdles of clinical timing and scale in our future work, paving the way for their ultimate translational application.

It must be admitted that the current research still has the following limitations. First, the printing of more complex structures containing multiple cell types may further enhance liver function. Second, although we found evidence of liver zonation, the mechanism by which it occurs remains unclear. Finally, the sample size varied across different experimental groups in this study. The Sham group was assigned the largest sample size ($n = 36$) to precisely establish baseline survival rates following ALF. While the cf-3DPT group ($n = 8$) served as an auxiliary control to exclude effects from the biomaterial itself, its sample size was determined based on ethical considerations and pre-experimental results. Despite sample size imbalance, the significant statistical difference in key intergroup comparisons (e.g. 3DPT vs Sham, $P = 0.008$) indicates that the primary conclusions are robust.

5. Conclusion

In conclusion, we achieved long-term large-scale expansion of PMHs with defined media and successfully constructed liver tissue using 3D bioprinting technology. 3D printed liver tissue prolongs the overall survival of mice with ALF, and its excellent liver function suggests great promise for clinical application in the future.

Data availability statement

The data cannot be made publicly available upon publication because no suitable repository exists for hosting data in this field of study. The data that support the findings of this study are available upon reasonable request from the authors.

Supplementary_Figs_Tables available at https://doi.org/10.1088/1758-5090/ae288d/data1.

Acknowledgment

This work was supported by Grants from Special clinical research project of Central High-Level Hospital of Peking Union Medical College Hospital (2022-PUMCH-B-034), China Postdoctoral Science Foundation (2022TQ0042), Beijing Natural Science Foundation (7212077), CAMS Innovation Fund for Medical Sciences (2021-I2M-1-058), Tsinghua University-Peking Union Medical College Hospital Cooperation Project (PTQH201904552), and National Natural Science Foundation of China (82300754、82472174).

Author contributions

Bao Jin
Conceptualization (lead), Visualization (lead), Methodology (lead), Investigation (lead), Writing – original draft (lead)

Zhibo Xie 0000-0001-5063-9070
Investigation (equal), Methodology (equal), Writing – review & editing (equal)

Yinhan Wang
Resources (equal), Investigation (equal), Writing – review & editing (equal)

Yuce Lu 0009-0004-4638-9178
Methodology (equal), Software (equal)

Lejia Sun
Software (supporting), Validation (supporting)

Zhangyuting He
Resources (supporting)

Yuqian Ye
Resources (supporting)

Zhiyuan Fang
Methodology (supporting)

Yarong Chi
Methodology (supporting)

Mingchang Pang
Methodology (supporting)

Changcan Li
Investigation (supporting)

Hang Sun
Investigation (supporting)

Zhuoran Danny Jiang 0000-0002-9548-4348
Investigation (supporting)

Xindi Ke
Investigation (supporting)

Haifeng Xu
Formal analysis (supporting)

Haitao Zhao
Formal analysis (supporting)

Xinting Sang
Formal analysis (supporting)

Shunda Du
Formal analysis (supporting)

Pengyu Huang
Supervision (equal), Conceptualization (equal)

Huayu Yang 0000-0001-9791-3559
Supervision (equal), Conceptualization (equal)

Yilei Mao 0000-0003-0449-4223
Supervision (equal), Conceptualization (equal)

References

[1] Michalopoulos G K and Bhushan B 2021 Liver regeneration: biological and pathological mechanisms and implications *Nat. Rev. Gastroenterol. Hepatol.* **18** 40–55
[2] Tong Y, Zhu Y and Cai X 2020 The origin of newborn hepatocytes in associating liver partition and portal vein ligation for staged hepatectomy (ALPPS)-derived regeneration *Hepatobiliary Surg. Nutr.* **9** 687–90
[3] Burra P, Samuel D, Sundaram V, Duvoux C, Petrowsky H, Terrault N and Jalan R 2021 Limitations of current liver donor allocation systems and the impact of newer indications for liver transplantation *J. Hepatol.* **75** S178–S190
[4] Dutkowski P, Linecker M, DeOliveira M L, Müllhaupt B and Clavien P A 2015 Challenges to liver transplantation and strategies to improve outcomes *Gastroenterology* **148** 307–23
[5] Dwyer B J, Macmillan M T, Brennan P N and Forbes S J 2021 Cell therapy for advanced liver diseases: repair or rebuild *J. Hepatol.* **74** 185–99
[6] Cao H *et al* 2012 Therapeutic potential of transplanted placental mesenchymal stem cells in treating Chinese miniature pigs with acute liver failure *BMC Med.* **10** 56
[7] Mazza G, Al-Akkad W, Rombouts K and Pinzani M 2018 Liver tissue engineering: from implantable tissue to whole organ engineering *Hepatol. Commun.* **2** 131–41
[8] Hosseini V, Maroufi N F, Saghati S, Asadi N, Darabi M, Ahmad S N S, Hosseinkhani H and Rahbarghazi R 2019 Current progress in hepatic tissue regeneration by tissue engineering *J. Transl. Med.* **17** 383
[9] Daly A C, Prendergast M E, Hughes A J and Burdick J A 2021 Bioprinting for the biologist *Cell* **184** 18–32
[10] Xie F, Xiao Y and Chen M 2020 Three-dimensional bioprinted liver tissue for transplantation: hope or hype? *Hepatobiliary Surg. Nutr.* **9** 788–90
[11] Noor N, Shapira A, Edri R, Gal I, Wertheim L and Dvir T 2019 3D printing of personalized thick and perfusable cardiac patches and hearts *Adv. Sci.* **6** 1900344
[12] Grigoryan B *et al* 2019 Multivascular networks and functional intravascular topologies within biocompatible hydrogels *Science* **364** 458–64
[13] Yang H *et al* 2021 Three-dimensional bioprinted hepatorganoids prolong survival of mice with liver failure *Gut* **70** 567–74
[14] Zhang K *et al* 2018 *In vitro* expansion of primary human hepatocytes with efficient liver repopulation capacity *Cell Stem Cell* **23** 806–19e4
[15] Xiang C *et al* 2019 Long-term functional maintenance of primary human hepatocytes *in vitro Science* **364** 399–402
[16] Peng W C *et al* 2018 Inflammatory cytokine TNFalpha promotes the long-term expansion of primary hepatocytes in 3D culture *Cell* **175** 1607–19e15
[17] Hu H *et al* 2018 Long-term expansion of functional mouse and human hepatocytes as 3D organoids *Cell* **175** 1591–1606e19
[18] Katsuda T, Kawamata M, Hagiwara K, Takahashi R-U, Yamamoto Y, Camargo F D and Ochiya T 2017 Conversion of terminally committed hepatocytes to culturable bipotent progenitor cells with regenerative capacity *Cell Stem Cell* **20** 41–55
[19] Wu H, Zhou X, Fu G-B, He Z-Y, Wu H-P, You P, Ashton C, Wang X, Wang H-Y and Yan H-X 2017 Reversible transition between hepatocytes and liver progenitors for *in vitro* hepatocyte expansion *Cell Res.* **27** 709–12
[20] Li B *et al* 2021 *In vitro* expansion of cirrhosis derived liver epithelial cells with defined small molecules *Stem Cell Res* **56** 102523
[21] Deng B *et al* 2024 Revitalizing liver function in mice with liver failure through transplantation of 3D-bioprinted liver with expanded primary hepatocytes *Sci. Adv.* **10** eado1550
[22] Mao S, He J, Zhao Y, Liu T, Xie F, Yang H, Mao Y, Pang Y and Sun W 2020 Bioprinting of patient-derived *in vitro* intrahepatic cholangiocarcinoma tumor model: establishment, evaluation and anti-cancer drug testing *Biofabrication* **12** 045014
[23] Bissig K-D, Le T T, Woods N-B and Verma I M 2007 Repopulation of adult and neonatal mice with human hepatocytes: a chimeric animal model *Proc. Natl Acad. Sci. USA* **104** 20507–11
[24] Ponder K P, Gupta S, Leland F, Darlington G, Finegold M, DeMayo J, Ledley F D, Chowdhury J R and Woo S L 1991 Mouse hepatocytes migrate to liver parenchyma and function indefinitely after intrasplenic transplantation *Proc. Natl Acad. Sci. USA* **88** 1217–21
[25] Myronovych A *et al* 2008 Role of platelets on liver regeneration after 90% hepatectomy in mice *J. Hepatol.* **49** 363–72
[26] Xie F *et al* 2021 Three-dimensional bio-printing of primary human hepatocellular carcinoma for personalized medicine *Biomaterials* **265** 120416
[27] Sun L *et al* 2020 Application of a 3D bioprinted hepatocellular carcinoma cell model in antitumor drug research *Front. Oncol.* **10** 878
[28] Sun W *et al* 2020 The bioprinting roadmap *Biofabrication* **12** 022002
[29] Ren Y *et al* 2021 Developments and opportunities for 3D bioprinted organoids *Int. J. Bioprint.* **7** 364
[30] Ma L, Wu Y, Li Y, Aazmi A, Zhou H, Zhang B and Yang H 2020 Current advances on 3D-bioprinted liver tissue models *Adv. Healthcare Mater.* **9** e2001517
[31] Xiao J *et al* 2019 Global liver disease burdens and research trends: analysis from a Chinese perspective *J. Hepatol.* **71** 212–21
[32] Byass P 2014 The global burden of liver disease: a challenge for methods and for public health *BMC Med.* **12** 159

[33] Sucher R and Sucher E 2020 Artificial intelligence is poised to revolutionize human liver allocation and decrease medical costs associated with liver transplantation *Hepatobiliary Surg. Nutr.* **9** 679–81
[34] Español–Suñer R, Carpentier R, Van Hul N, Legry V, Achouri Y, Cordi S, Jacquemin P, Lemaigre F and Leclercq I A 2012 Liver progenitor cells yield functional hepatocytes in response to chronic liver injury in mice *Gastroenterology* **143** 1564–75e7
[35] Basma H *et al* 2009 Differentiation and transplantation of human embryonic stem cell-derived hepatocytes *Gastroenterology* **136** 990–9
[36] Touboul T *et al* 2010 Generation of functional hepatocytes from human embryonic stem cells under chemically defined conditions that recapitulate liver development *Hepatology* **51** 1754–65
[37] Takayama K *et al* 2012 Generation of metabolically functioning hepatocytes from human pluripotent stem cells by FOXA2 and HNF1alpha transduction *J. Hepatol.* **57** 628–36
[38] Huang P, He Z, Ji S, Sun H, Xiang D, Liu C, Hu Y, Wang X and Hui L 2011 Induction of functional hepatocyte-like cells from mouse fibroblasts by defined factors *Nature* **475** 386–9
[39] Huang P *et al* 2014 Direct reprogramming of human fibroblasts to functional and expandable hepatocytes *Cell Stem Cell* **14** 370–84
[40] Kuo T K, Hung S, Chuang C, Chen C, Shih Y V, Fang S Y, Yang V W and Lee O K 2008 Stem cell therapy for liver disease: parameters governing the success of using bone marrow mesenchymal stem cells *Gastroenterology* **134** 2111–21.e3
[41] Levy G, Bomze D, Heinz S, Ramachandran S D, Noerenberg A, Cohen M, Shibolet O, Sklan E, Braspenning J and Nahmias Y 2015 Long-term culture and expansion of primary human hepatocytes *Nat. Biotechnol.* **33** 1264–71
[42] Nguyen M P, Jain V, Iansante V, Mitry R R, Filippi C and Dhawan A 2020 Clinical application of hepatocyte transplantation: current status, applicability, limitations, and future outlook *Expert Rev. Gastroenterol. Hepatol.* **14** 185–96
[43] Shibuya K, Watanabe M, Goto R, Zaitsu M, Ganchiku Y and Taketomi A 2021 The efficacy of the hepatocyte spheroids for hepatocyte transplantation *Cell Transplant.* **30**
[44] Paris J and Henderson N C 2022 Liver zonation, revisited *Hepatology* **76** 1219–30
[45] Panday R, Monckton C P and Khetani S R 2022 The role of liver zonation in physiology, regeneration, and disease *Semin. Liver Dis.* **42** 001–016